Potential for Energy Recovery from Boundary Layer Ingesting Actuator Disk Propulsion

Ngonidzashe.E. Mutangara[*], Lelanie. Smith[†], Kenneth.J. Craig[‡]
University of Pretoria, Pretoria, South Africa, 0001

Drewan.S. Sanders[§]
Cranfield University, Bedford, United Kingdom, MK43 0AL

The theoretical benefits of highly integrated propulsion systems are highlighted herein by assessing the potential for energy recovery utilization using actuator disk propulsion. Decomposing aerodynamic forces into thrust and drag for closely integrated bodies, particularly those employing boundary layer ingestion, becomes challenging. In this work, a mechanical energy-based approach was taken using the power balance method. This allowed the performance to be analyzed through the mechanical flow power in the fluid domain, disregarding the need for any explicit definition of thrust and drag. Through this, the benefit of boundary layer ingestion was observed from a wake energy perspective as a decrease in the downstream mechanical energy deposition and associated viscous dissipation. From a propulsion perspective, the reduction in power demand necessary to produce propulsive force indicated the possibility of power savings by utilizing the energy contained within the ingested boundary layer flow.

[*]MEng Student, Department of Mechanical and Aeronautical Engineering; ngonidzashe.e.mutangara@cranfield.ac.uk Student Member AIAA (Corresponding Author).
[†]Senior Lecturer, Department of Mechanical and Aeronautical Engineering; lelanie.smith@up.ac.za. Member AIAA.
[‡]Professor, Department of Mechanical and Aeronautical Engineering; ken.craig@up.ac.za.
[§]Research Fellow, School of Aerospace, Transport and Manufacturing; d.s.sanders@cranfield.ac.uk Member AIAA.

Nomenclature

S_{ref} = reference area [m^2]

ρ = fluid density [kg/m^3]

c = chord length [m]

u, v, w = perturbation velocities [m/s]

p = static pressure [Pa]

$\hat{\boldsymbol{n}}$ = unit normal vector, out-of-control volume

x, y, z = cartesian axes

Re = Reynolds number

M = Mach Number

$\boldsymbol{V}$ = fluid velocity $(V_\infty + u)\hat{x} + v\hat{y} + w\hat{z}$

V^2 = fluid speed squared $= \boldsymbol{V} \cdot \boldsymbol{V}$

V_n = side cylinder normal velocity $vn_y + wn_z$

$\bar{\boldsymbol{\tau}}$ = viscous stress tensor

$\mathbf{F}_B$ = integrated force acting on the body's surfaces by the fluid [N]

$\mathbf{F}_P$ = propulsor force [N]

F_x = net streamwise force in x

$\dot{E}_a$ = axial kinetic energy deposition rate [W]

$\dot{E}_v$ = transverse kinetic energy deposition rate [W]

$\dot{E}_p$ = pressure-work deposition rate [W]

$\dot{E}_\tau$ = rate of viscous boundary work [W]

Θ = volumetric power [W]

$\dot{\varepsilon}_{prop}$ = kinetic energy inflow rate [W]

$\dot{\varepsilon}$ = mechanical energy outflow rate [W]

Φ = deposition rate [W]

dS = surface element of the control volume

dV = volume element of the control volume

γ = climb angle [°]

η_{prop} = propulsive efficiency

Γ = climb rate [m/s] $= V_\infty \sin\gamma$

W = aircraft weight [N]

Subscripts

m = recoverable mechanical-energy quantity

B = on body surface quantity

P = propulsor surface quantity

ref = reference quantity

TE = trailing-edge quantity

Φ = power balance quantity

∞ = freestream quantity

O = outer control volume surface

TP = transverse-plane

SC = side-cylinder

Superscripts

$'$ = quantity for non-boundary layer ingesting configuration

I. Introduction

Boundary Layer Ingestion (BLI) promises to improve overall aircraft aerodynamic efficiency through favorable integration of the propulsion system within the airframe. In its simplest description, the propulsion system is incorporated towards the rear of the airframe, where it ingests the boundary layer flow that has developed over the preceding aerodynamic surfaces. BLI has been studied on various airframe types, including conventional tube-and-wings [1–3], wide-body lifting fuselages [4–12], and Blended-Wing-Bodies [13–19], with each claiming various levels of benefit. However, despite numerous research efforts, there remain uncertainties regarding the true benefit attainable from BLI as a mechanism alone. A primary cause of this uncertainty is the challenge in performance accounting introduced by the close aerodynamic coupling between the airframe and propulsion system. This is because

distinctions between thrust and drag become ambiguous since the underlying assumptions behind typical performance accounting conventions [20,21] become invalid.

Thrust as a concept has great significance because it is not merely a simple division of net vehicle force but rather represents the useful work done by the propulsion system [22]. Understanding and quantifying the useful work done by a system versus the total power supplied enables efficiencies to be defined and provides a consistent means of comparison between competing designs at a system level. Propulsive efficiency has been an essential metric for comparing conventional podded engine installations [23,24]. However, unlike freestream ingesting propulsion systems assumed to be aerodynamically decoupled, BLI does not allow for a valid definition of thrust that corresponds meaningfully to useful work due to the significant interaction between the airframe and propulsor flowfields. As such, previously useful metrics like propulsive efficiency also become invalid, as is evident from various works which have demonstrated BLI propulsive efficiencies over 100% [25–27]. These references, i.e., [25–27], each identify that the conventional propulsive efficiency definition describes the ratio of energies between the useful propulsive work done to produce thrust and the total energy imparted to the flow.

A limitation of this definition is exposed when applied to configurations other than freestream ingesting designs, particularly those inducting boundary layer flow. In the case of BLI configurations, a part of the energy within the wake, usually imparted to the flow and irreversibly lost to the surroundings for free stream ingesting designs, becomes available to the propulsor to produce thrust in addition to the delivered shaft power. This leads to a scenario where the available propulsive power exceeds the energy imparted to the flow resulting in an efficiency, i.e., η_{prop}, greater than 100%.

At first glance, this result seemingly defies both the second law of thermodynamics and the requirement for energy conservation, as efficiencies *strictly* cannot exceed 100%. However, this outcome merely highlights the inadequacy of the current propulsive efficiency definition when applied to highly integrated configurations.

The implications of being unable to define useful work in the form of thrust are twofold, with both aspects contributing to the uncertainties and disparities of benefits reported in literature. Firstly, erroneous interpretations regarding the underlying reasons or mechanisms behind BLI benefits emerge. Concepts such as drag reduction/mitigation and increased propulsive efficiency are invalid as they breach the very assumptions upon which they have been defined. Secondly, no system-level (or propulsion-level) metrics uniquely allow for a direct, consistent, and fair comparison between non-BLI and BLI propulsion systems, demonstrated by Hall et al. [28]. Subsequently, most studies have

resorted to some form of the Power Saving Coefficient first defined by Smith [29], which compares the power of a BLI configuration versus a podded (freestream ingesting) design. The result is that the reported benefits highly depend on the baseline podded configuration selected for the comparison. This introduces uncertainty about the overall benefit achieved and to what degree that benefit may be attributed to BLI as a mechanism.

To try and overcome these challenges, Drela [30] proposed an alternative control volume approach that examines the aerodynamic performance from a mechanical energy-based perspective. This is commonly referred to as the Power Balance Method (PBM), and its main advantage is that it is independent of distinguishing between thrust and drag. Instead, it traces how the power supplied by the aircraft is consumed aerodynamically in the surrounding flow field [31]. Moreover, Sanders and Laskaridis [22] expand on the idea by showing how the formulations of the PBM represent aircraft aerodynamics from the absolute reference frame (ARF). In the ARF, the aircraft moves through the initially undisturbed atmosphere rather than the relative reference frame (RRF), which views the aircraft as motionless with the flow of the atmosphere passing over it. This has significance because work and energy relationships are reference frame dependent, and the ARF perspective views all aerodynamic power as emanating from the aircraft, which is then consumed by the atmosphere. This is preferred over the RRF, which can be considered in a similar vein to a wind tunnel setup, where part of the aerodynamic power is supplied "externally" by the flow field (or wind tunnel fan in this analogy). Therefore, the ARF makes it easier to study how energy is transferred from one mechanism to another in a causal manner, helping improve the interpretations of the underlying mechanisms of BLI propulsion.

From the ARF perspective, aerodynamic surfaces are viewed as imparting energy to the flow via the no-slip condition. The wake behind a simple aerodynamic body is considered an excess of mechanical energy rather than a deficit. As a result, the mechanism behind BLI benefit is regarded as one whereby the propulsor can harvest some of the available mechanical energy left in the wake while simultaneously counteracting the net streamwise force. This is considered wake attenuation and aids in preventing viscous dissipation of available excess mechanical energy downstream of the aircraft. Based on this concept, the wake of an unpowered aerodynamic body can be studied in terms of available mechanical energy, where a Potential for Energy Recovery (PER) metric is defined, quantifying the theoretical limit of benefit attainable from BLI [22]. The Power Balance Method helps address the two challenges mentioned above. Firstly, the causality viewed from the ARF improves the identification and interpretation of the underlying BLI mechanism of benefit as a form of harvesting mechanical energy from the flow. Secondly, the PER metric sets a maximum theoretical benefit limit for a given aerodynamic body independent of a baseline propulsion system.

In a previous paper [32], the concept of PER was demonstrated and explored for different isolated aerodynamic bodies, including a flat plate, NACA0012 airfoil, and two bodies of revolution, namely the Myring and F-57 low drag bodies. The PER analysis revealed that the drag power available at the trailing edge in the form of mechanical energy ranged between 9% to 12%. However, as PER estimates the maximum theoretical limit of the attainable savings through BLI, this paper explores to what degree this limit can be achieved using an ideal propulsive device. To do so, this study uses an actuator disk positioned at the trailing edge of each aerodynamic body, which ingests the entirety of the viscous wake while counteracting the net streamwise force to varying degrees. The wake behind the actuator disk is compared against that of an unpowered aerodynamic body to ascertain the reduction in wake dissipation and amount of mechanical energy harvesting to verify the PER.

Although the PSC metric primarily depends on the chosen freestream reference configuration, its use for BLI benefit assessment is still valuable through carefully considering its application. For instance, for simple retrofit BLI designs, such as those examined in this work, no significant modifications are made to the baseline freestream ingesting airframe to accommodate integration with the boundary layer ingesting propulsor (BLIP). For this scenario, the associated BLI power savings can be assessed by comparing the BLIP power against an ideal freestream ingesting propulsor having no internal losses and operating at a propulsive efficiency of 100%. The limiting case of an ideal BLIP which perfectly attenuates the ingested flow and fully utilizes the energy within the fluid, would report power savings equal to the theoretical maximum indicated via PER. Appendix 0 provides this relationship between PSC and PER in more detail for the reader's convenience.

This work takes a novel approach utilizing the PBM by employing the ARF perspective to assess the PER using an ideal propulsor representation numerically in RANS CFD. The study's contribution is offered by investigating ways BLI benefits can be evaluated using energy-based methods. The performance metrics of interest in this study included the energy-based loss variation coefficient (LVC) [31], which tallies the difference in downstream mechanical energy losses between a freestream and boundary layer ingesting configuration. Also included was the power saving coefficient (PSC) [29,33–36], which compares the relative power consumption between freestream and boundary layer ingesting designs. Lastly, the potential for energy recovery (PER) [22] and exergy waste coefficient (E_xWC) [19,37–39] were considered, which provide the theoretical maximal power savings obtainable through BLI by utilizing available mechanical energy within the flow in the instance of PER and exergy (i.e., mechanical + thermal energy) in

the case of E_xWC. The impact of this research is to impart an alternative approach to interpreting and understanding BLI mechanisms and calibrating expectations of the benefits truly achievable by more complex BLI installations.

II.Mathematical Models and Numerical Methodology

A.Mechanical Energy Methods

Mechanical energy analysis through the PBM [30] provides an alternate means of understanding and analyzing aircraft performance. Unlike nearfield methods, which offer a binary drag definition, i.e., pressure and skin friction, mechanical energy methods extend this understanding via an extensive decomposition into the various physical mechanisms which collectively contribute toward drag. Notably, a helpful approach is to view the flow field from an Absolute Reference Frame (ARF) perspective [22], whereby the aircraft is considered as moving through the air instead of the air moving over the aircraft. From this viewpoint, causality is introduced whereby power is transferred to the flow via the no-slip condition along aerodynamic surfaces. This power is then consumed through various flow structures that arise during the vehicle's motion.

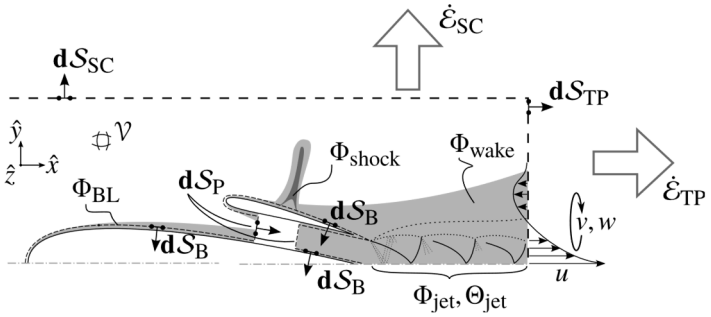

Figure 1 2D cutaway view of 3D Control Volume surrounding an aerodynamic body adapted from [22]**. Copyright © 2020 by Drewan S. Sanders and Panagiotis Laskaridis. Adapted with permission**

These mechanisms are indicated in Figure 1 and show the mechanical energy crossing the control volume boundaries via the Trefftz Plane ($\dot{\varepsilon}_{TP}$) and side cylinders ($\dot{\varepsilon}_{SC}$) as the body moves through the fluid. Within the control volume are shaded regions depicting the boundary layers, shocks, wake, and jet regions which contribute volumetrically towards a part of the mechanical energy through pressure-volume work (Θ) and viscous dissipation (Φ). A significant advantage of mechanical energy methods is their applicability to wake energy management and recovery. This is granted through their ability to trace the evolution of energies and accumulation of dissipation downstream of the airframe. Near the configuration trailing edge, mechanical energy is deposited into the wake and later dissipated downstream to the surroundings. This characteristic intuitively introduces the concept of energy recovery, where the

objective of mechanisms such as BLI would be to utilize the deposited mechanical energy within the wake before it is irreversibly lost to the surroundings. This benefit may be described symptomatically as the prevention of mechanical energy dissipation within the wake.

1. Performance Assessment Parameters: Potential for Energy Recovery and Power Saving Coefficient

For mechanical energy analyses, the total flight power can be predicted by estimation of the power outflow via various physical processes, and through this, the power out- and inflow requirements can be obtained using the relation, $P_{available} = P_{required} + W\Gamma$, formally provided in equation (1). Usually, for both powered and unpowered adiabatic flows, the rate of viscous boundary work (i.e., $\dot{E}_\tau$) is assumed to be negligible and can be omitted from the formulation.

$$P_K = \dot{E}_a + \dot{E}_v + \dot{E}_p + \dot{E}_w + \dot{E}_\tau + \Phi + \Theta \underbrace{- \overbrace{(\boldsymbol{F}_P + \boldsymbol{F}_B)}^{\boldsymbol{NAF}} \cdot \boldsymbol{V}_\infty}_{W\Gamma} \tag{1}$$

The power-saving coefficient (PSC) [29], as stated in equation (2)(a), is exclusively reserved for the quantification of BLI benefits for powered configurations. The PSC evaluates the difference in power between a non-BLI $(P_K{}')$, and BLI propulsor (P_K) required to produce a specific net streamwise force (F_x), i.e., the x-component of the net assembly force (NAF). F_x can be determined either from a nearfield integration of the shear stresses and pressures along the airframe and propulsor surfaces or from a far-field wake integration. The studies conducted herein provide F_x via a far-field integration using the expression provided in equation (2)(b).

$$PSC \equiv \frac{P_K{}' - P_K}{P_K{}'} = 1 - \frac{P_K}{P_K{}'} \qquad (a)$$

$$F_x = \iint -[(p - p_\infty) + \rho u(V_\infty + u)\, dS_O^{TP}] + \iint -\rho u V_n\, dS_O^{SC} \qquad (b) \tag{2}$$

The PSC can be obtained by comparing configurations with propulsors having either similar mechanical energy inflow, propulsive efficiency, jet velocity, area, or mass flow rate [28]. When considering entire aircraft, difficulties arise in effectively ranking the benefits of BLI using the PSC, as it relies heavily on the aerodynamic and propulsive characteristics of the chosen reference freestream ingesting configuration (FIC). Even if a standard reference configuration is considered, the PSC becomes misleading as power reduction benefits not directly associated with BLI, such as fuselage and wing design, may be accounted for within the PSC. Additionally, if the chosen reference is inefficient, an overly optimistic interpretation of the advantages of BLI is obtained. A fair comparison instead would compare the performance of a fully optimized BLIC with a fully optimized FIC [40].

Conceptually, this is done by assuming the podded and BLI variants are powered by equivalently ideal propulsors. In this instance, the BLIP perfectly attenuates the boundary layer/wake energy without affecting the upstream flow or depositing any energy downstream while propelling the body. At cruise, these propulsors would provide thrust equal to the airframe drag and power inflow equal to the drag power. Through this, it is possible to provide a theoretical maximum limit of power savings, which for *incompressible* flows, can be assessed through PER [22]. This metric quantifies the potential for aerodynamic improvement by tracking the mechanical energy losses observable as various forms of dissipation depicted in equation (4). Additionally, PER can easily be related to mechanical energy ($\dot{E}_m = \dot{E}_K + \dot{E}_p$) via a recasting of equation (1) for unpowered configurations (UC) in steady-level flight illustrated through equations (3) – (5), giving the complement of PER, i.e., (PER^c) as provided in [32].

As the FIP becomes more ideal

$$\lim_{P_K' \to \text{ideal}} P_K' \Big|_{F_x = 0} = \boldsymbol{F}_P \cdot \boldsymbol{V}_\infty = \boldsymbol{F}_B \cdot \boldsymbol{V}_\infty \,, \tag{3}$$

and as the BLIP becomes more ideal

$$\lim_{P_K \to \text{ideal}} P_K \Big|_{F_x = 0} = \Phi_{\text{airframe}} = \sum \Phi_i = \underbrace{\Phi_{\text{surf}} + \Phi_{\text{wake}}}_{\Phi_p} + \cancel{\Phi}_{\text{vortex}} + \cancel{\Phi}_{\text{wave}} \,. \tag{4}$$

Comparing the ideal FIP and BLIP performance then yields

$$\begin{aligned} \therefore PSC_{\text{ideal}} = PER_{\text{airframe}} &\equiv \frac{\boldsymbol{F}_B \cdot \boldsymbol{V}_\infty - \Phi_{\text{airframe}}}{\boldsymbol{F}_B \cdot \boldsymbol{V}_\infty} \\ &= 1 - \frac{\Phi_{\text{airframe}}}{\boldsymbol{F}_B \cdot \boldsymbol{V}_\infty} = \frac{\dot{E}_m}{\boldsymbol{F}_B \cdot \boldsymbol{V}_\infty} = PER^c_{\text{airframe}} \end{aligned} \tag{5}$$

It is possible to arrive at the same expression in equation (5) via an alternative means by recasting the mechanical energy loss formulation provided by Sato [31] for an isolated airframe in incompressible flow, as shown in equation (6). From this, it is possible to show that the mechanical energy loss (Φ^*) becomes quite advantageous as it lends more insight into what PER quantifies, as well as provides a clear view of the source of the benefit of boundary layer/wake ingesting systems from a wake energy management perspective.

$$\Phi^* = \sum \dot{E} + \sum \Phi + \sum \not{\emptyset}^{=0,\ \text{incompressible flow}} = \boldsymbol{F}_B \cdot \boldsymbol{V}_\infty$$

$$\Rightarrow 1 - \left(\frac{\sum \Phi}{\Phi^*}\right)_{\text{airframe}} = \left(\frac{\sum \dot{E}}{\Phi^*}\right)_{\text{airframe}} \equiv PER_{\text{airframe}} = PER^c_{\text{airframe}} \tag{6}$$

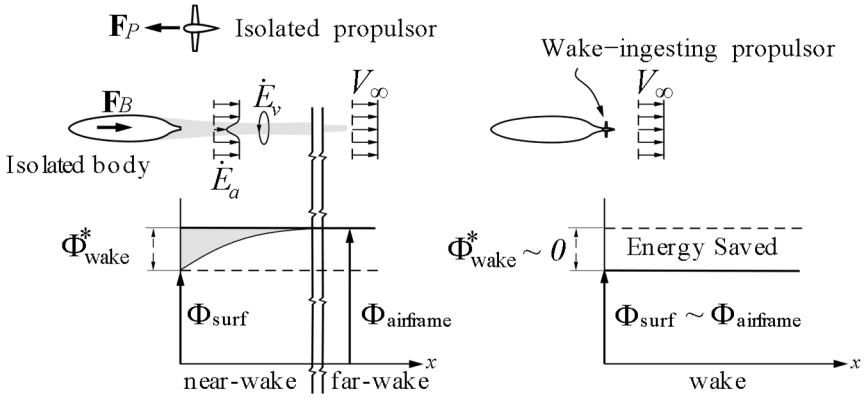

Figure 2 Comparison of dissipation in isolated (left) and wake-ingesting (right) propulsors for a 2D airfoil

The illustration in Figure 2, as well as equation (7), makes it possible to show that the benefits observed for boundary layer/wake ingesting systems originate from a reduction in profile mechanical losses $\left(\Phi_p^*\right)$ by utilizing mechanical energy which would have otherwise dissipated downstream.

$$\boldsymbol{F}_B \cdot \boldsymbol{V}_\infty = \Phi^*_{\text{airframe}} = \sum \Phi_i^* = \underbrace{\Phi^*_{\text{surf}} + \Phi^*_{\text{wake}}}_{\Phi_p^*}$$

$$\Rightarrow 1 - \frac{\Phi^*_{\text{surf}}}{\Phi^*_{\text{airframe}}} = \frac{\Phi^*_{\text{wake}}}{\Phi^*_{\text{airframe}}} = \frac{\sum \dot{E}_{\text{wake}} + \sum \Phi_{\text{wake}}}{\Phi_p^*} \equiv PER_{\text{max, airframe}} \tag{7}$$

The wake energy content of powered BLIC can be represented by recasting equation (1) for steady flight conditions, as shown in equation (8). However, to prevent misinterpretation of this energy as being recoverable, it will instead be referred to as energy waste coefficient (E_nWC), a reduced form of Arntz's [19,37–39] exergy waste coefficient (E_xWC) applied to incompressible flows with negligible thermal energy contributions.

$$P_K - W\Gamma = \sum \Phi_i^* = \Phi^*_{\text{surf}} + \Phi^*_{\text{wake}} + \Phi^*_{\text{P}}$$

$$\Rightarrow 1 - \left(\frac{\Phi^*_{\text{surf}} + \Phi^*_{\text{P}}}{P_K - W\Gamma}\right) = \frac{\Phi^*_{\text{wake}}}{P_K - W\Gamma} = \frac{\sum \dot{E}_{\text{wake}} + \sum \Phi_{\text{wake}}}{P_K - W\Gamma} \equiv E_n WC_{\text{max, powered}} \tag{8}$$

2. Performance Assessment Parameters

Performance evaluation of highly integrated configurations becomes particularly challenging primarily when assessed via force-based metrics such as the profile drag (D_p). This is because the pressure interaction between the coupled bodies strongly affects profile drag. As a result, individual forces acting on these bodies cannot be used to provide insight into the viscous drag [4,10] or thrust when BLICs are considered. Energy-based methods offer an alternative means of assessment through dissipation, which is not explicitly affected by local changes in pressure gradient [4,10]. To highlight these differences in the various case studies, the force-based drag variation coefficient (DVC) is compared against the energy-based loss variation coefficient (LVC) given in equations (9)(a) and (b), respectively.

$$\text{LVC} \equiv \frac{\Phi_p^{*\prime} - \Phi_p^*}{\Phi_p^{*\prime}} \qquad (a)$$

$$\text{DVC} \equiv \frac{D_p{}' - D_p}{D_p{}'} \qquad (b) \tag{9}$$

Additional non-dimensional performance parameters used include the streamwise force and power coefficients shown in equations (10)(a) and (b), respectively. The streamwise force coefficient provided the non-dimensional resultant force acting over the aerodynamic configuration, representing the conventional drag coefficient for an unpowered design. On the other hand, the power coefficient was used to describe the energy-based non-dimensional mechanical inflow and outflow powers expressed through P_K and P_Φ.

$$CF_x = \frac{F_x}{\frac{1}{2}\rho_\infty V_\infty^2 A_{ref}} \qquad (a)$$

$$CP = \frac{P}{\frac{1}{2}\rho_\infty V_\infty^3 A_{ref}} \qquad (b) \tag{10}$$

B. Powered Configuration Numerical Modelling and Analysis Considerations

The unpowered studies conducted in [32] were extended in this work to include propulsion, modeled using an actuator disk (AD) [41]. For average-fidelity modeling of propulsion systems such as turbofans, pressure-drop interface ADs are satisfactory for approximating the propulsor impact on a flow field [38].

Each analysis was modeled with an AD sized to sufficiently ingest the entire boundary layer and illustrate the BLI wake-filling effects. Specific operating conditions were chosen for visualization via contours of the perturbation velocity magnitude defined in equation (11). Hereafter, the pressure jump was varied to achieve an array of net streamwise force conditions wherein the PSC and E_nWC were evaluated.

$$\left|\boldsymbol{V}_{pertubation}\right| = |\boldsymbol{V} - \boldsymbol{V}_{\infty}| \tag{11}$$

C.Geometric models and analysis Boundary Conditions

Isolated Propulsor: The freestream propulsor was modeled as an actuator disk within a circular computational domain based on work presented in [32] with a diameter of 16 chords based on a NACA 0012 airfoil of 1m chord (c = 1m). The study isolates the energy analysis to the control volume (CV) surrounding the propulsor, i.e., CV-II, in Figure 3(a), with the thrust being set to balance the drag of a hypothetical body sufficiently decoupled from the propulsor. In contrast, initial studies conducted in [32] consider the same decoupling but instead focus on the unpowered aerodynamic body in CV-I.

NACA 0012 Airfoil: The study primarily extends from the unpowered non-lifting (α = 0deg) NACA 0012 airfoil study in [32], which is modified to include a propulsor at the aft body as illustrated in Figure 3(b) and modeled using a pressure jump AD. The boundary conditions were similarly obtained from the numerical study conducted by Jespersen et al. [42]. The flow was assumed as steady and incompressible with a freestream M_∞ = 0.15 and Re = 6×10^6 based on the airfoil chord of 1m.

Bodies of Revolution (BoR): Myring Low-Drag (MLDB) and F-57 Low-Drag Bodies: Similarly, as done prior, the unpowered studies in [32] were modified by placing an AD propulsor at the trailing edge of the aft body. The MLDB flow was assumed as steady and incompressible with a Re = 10^7 and M_∞ = 0.06, as given in the literature [43]. The F-57 flow was also considered steady and incompressible (M_∞ = 0.04), with a constant velocity inlet condition of 15.24 m/s, yielding a Reynolds number based on body length (1.219m) of 1.2×10^6, as given in the work by Patel and Lee [44].

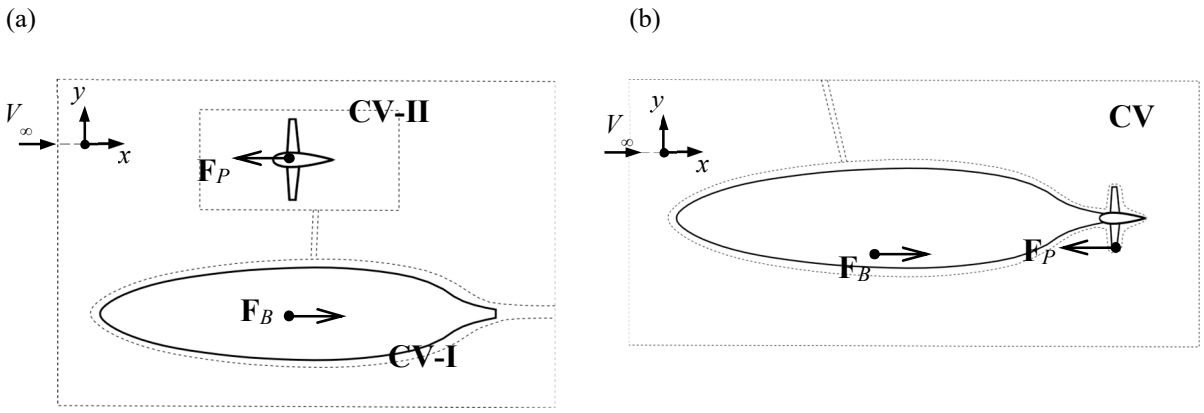

Figure 3 Control volume around (a) decoupled and (b) coupled powered configurations

III.Benchmarking of CFD Models

A. Application of Energy Methods on an isolated Actuator disk

The propulsor was sized to sufficiently ingest the entire boundary layer of an unpowered NACA 0012 airfoil with the geometric and freestream conditions mentioned in Section II-C. To verify the propulsor model and analysis approach for extracting powers and thrust using the PBM, a balance of power in- (P_K) and outflow (P_Φ) was tallied using the simplified mechanical energy formulation in equation (12). Additionally, as the propulsor model was based on momentum actuator disk theory (ADT), the relevant thrust was alternatively obtained via the product of the actuator disk area and proposed pressure jump, as indicated in equation (13). The propulsor power was then obtained by multiplying the calculated thrust by the average AD velocity.

$$\underbrace{\dot{E}_m + \Phi - \boldsymbol{NAF}\cdot\boldsymbol{V}_\infty}_{P_\Phi} = \underbrace{\iint\left[(p-p_\infty)+\frac{1}{2}\rho(V^2-V_\infty^2)\right]\boldsymbol{V}\cdot\boldsymbol{n}\,dS_B}_{P_K} \tag{12}$$

$$P_{AD} = \underbrace{\frac{1}{2}\left(\boldsymbol{V}_{\text{upstream}}+\boldsymbol{V}_{\text{downstream}}\right)}_{\boldsymbol{V}_{\text{avg}}}\cdot\underbrace{\Delta p\boldsymbol{A}}_{\boldsymbol{F}_P} \tag{13}$$

$$\eta_{\text{prop}} = \frac{P_{\text{propulsive power}}}{P_{\text{mechanical energy inflow rate}}}$$

$$= \frac{2}{1+\sqrt{C_T+1}} = \frac{2}{1+\frac{V_{\text{downstream}}}{V_{\text{upstream}}}} \equiv \eta_{\text{prop, AD}} \text{ where } C_T = \frac{\boldsymbol{F}_P}{\frac{1}{2}\rho V^2\boldsymbol{A}} \tag{14}$$

$$= \frac{P_K - \Phi_{\text{jet}}}{P_K} = 1 - \frac{\Phi_{\text{jet}}}{P_K} \equiv \eta_{\text{prop, PBM}}$$

Lastly, the AD propulsive efficiency (η_{prop}) was also compared via the definitions provided in ADT and the PBM shown in equation (14). This expression indicates that the propulsive power (useful work) is represented as the difference between the mechanical energy inflow rate (P_K) and the jet dissipative losses (Φ_{jet}).

Table 1 Freestream Propulsor Wake Energy Analysis: Coefficients of Net streamwise force, Mechanical Energy flow rate, and Power Balance solutions

Analysis	*Net streamwise Force*	*Net Propulsor Mechanical Energy Flow Rate & propulsive efficiency*	*Power Balance*	
	CF_x	CP_K (η_{prop})	CP_Φ	$\lvert CP_\Phi - CP_K\rvert$ (%Δ)
CFD	-9.66×10^{-3}	1.017×10^{-2} (0.99)	1.006×10^{-2}	1×10^{-4} (1.0%)
ADT	-9.65×10^{-3}	1.019×10^{-2} (0.99)		

The energy-based representation of η_{prop} is primarily identical to conventional definitions and thus still suffers from the same thrust/drag definition ambiguity for HICs. This is due to the surface definition of S_B, which is necessary for evaluating P_K (and, by extension, the propulsive power). This value is not unique and may be represented in multiple ways depending on the chosen force accounting method [45]. Therefore, this propulsive efficiency definition will only be used in this study with isolated propulsors where it is known to be strictly correct.

The AD was provided with a pressure jump (Δp) of 700Pa and, based on its dimensions h/c = 4% (**A**= 0.04m^2), gave a net streamwise force coefficient in the *thrust direction* within 0.2% of the ADT value as shown in Table 1. The power coefficients (i.e., CP_K and CP_Φ) also showed good agreement with their values within 1%. Figure 4(a) shows that the AD effectively accelerates the incoming flow in the streamwise direction by introducing a discontinuous pressure perturbation across its interface to produce thrust. This is shown in Figure 4(b) through the decrease in pressure boundary work $C\dot{E}_p$ and a corresponding increase in kinetic energy $C\dot{E}_k$ downstream of the AD.

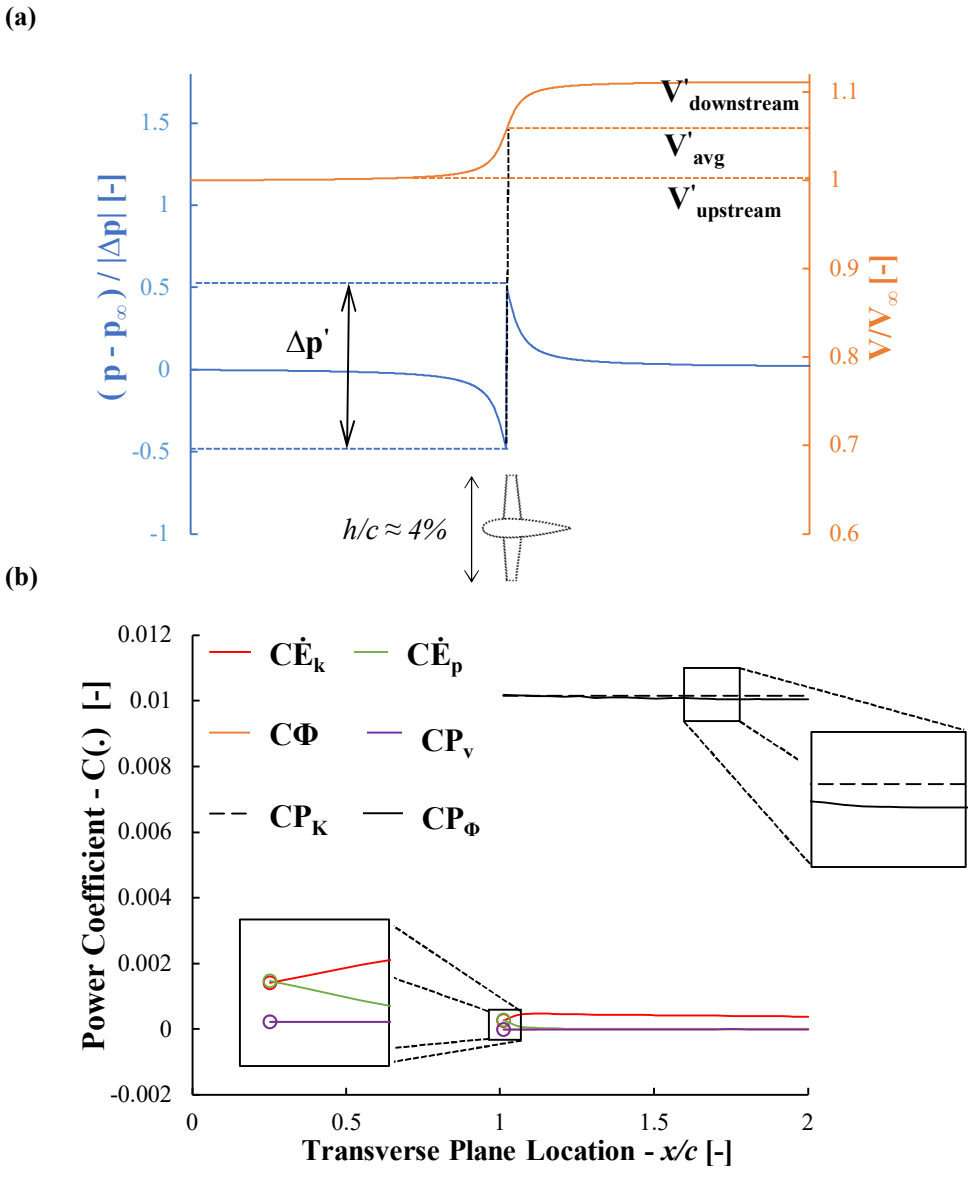

Figure 4 (a) Axial distribution of normalized static pressure and velocity (b) wake energy decomposition downstream of the AD

B. NACA0012 Powered configuration wake energy analysis

1. Validation of the Power Balance Formulation: NACA 0012 Airfoil

The unpowered NACA 0012 airfoil in [32] was modified to include a propulsor at x/c = 1.05. The AD was provided with the same pressure jump specified in Section III-A, which gave a net streamwise force of $CF_x = -2.93\times10^{-4}$ for the integrated configuration. Table 2 shows that the net streamwise force obtained is relatively close to the cruise condition (i.e., $CF_x = 0$). As a result, this operating point can provide an overview of what may be expected near cruise in terms of wake attenuation benefit from the integrated propulsor.

The sum of the wake energies (i.e., power outflow from the PBM) is compared against the net propulsor mechanical energy flow rate, as shown in Table 2, to verify the numerical implementation. The reported values indicate good agreement with <1% error between the power-in and outflow quantities.

Table 2 NACA 0012 airfoil Wake Energy Analysis: Net streamwise force, Mechanical Energy flow rate, and Power Balance solutions

Net Streamwise Force	*Net Propulsor Mechanical Energy Flow Rate*	*Power Balance*	
CF_x	CP_K	CP_Φ	$\lvert CP_\Phi - CP_K \rvert / (\%\Delta)$
-2.93×10^{-4}	8.116×10^{-3}	8.134×10^{-3}	1.74×10^{-5} ($\approx 0.2\%$)

An analysis of the evolution of mechanical energy downstream of the airfoil trailing edge is also provided in Figure 5, giving more insight into the propulsor wake attenuation. Examining the unpowered and powered BLIC in Figure 5 and Figure 6, the decrease in the downstream mechanical energy occurs due to the propulsor reducing the magnitude of velocity perturbations within the wake as it actively imparts kinetic energy to the flow. This leads to an appreciable attenuation of wake kinetic energy, shown through the significant decrease in $C\dot{E}_k$ in Figure 5.

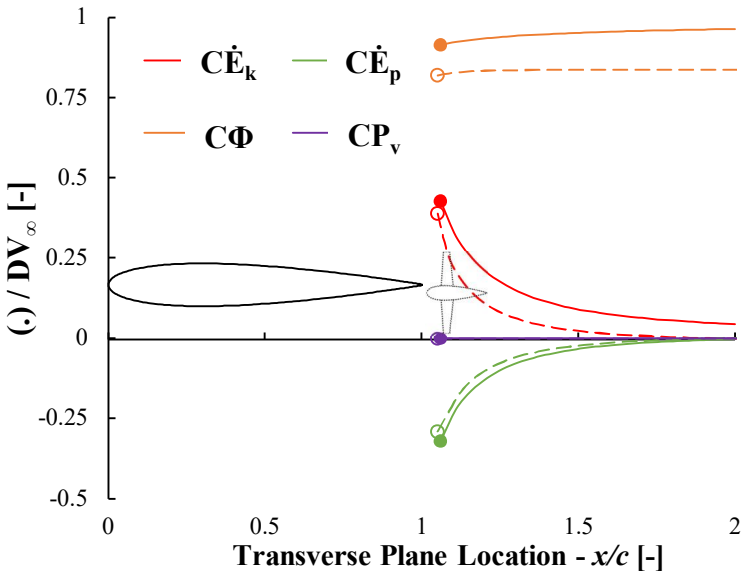

Figure 5 Energy loss rate and dissipation components as a function of Transverse Plane location for an unpowered (− solid) and BLI (− − dashed) NACA 0012 Airfoil

Additionally, the pressure field is modified due to the pressure-velocity coupling, which slightly reduces the intensity of the pressure-boundary work ($C\dot{E}_p$) shown in Figure 5. The lower wake energy decreases velocity gradients in the wake and shear layer regions, reducing the viscous dissipation as less work is required to dampen the downstream perturbative disturbances.

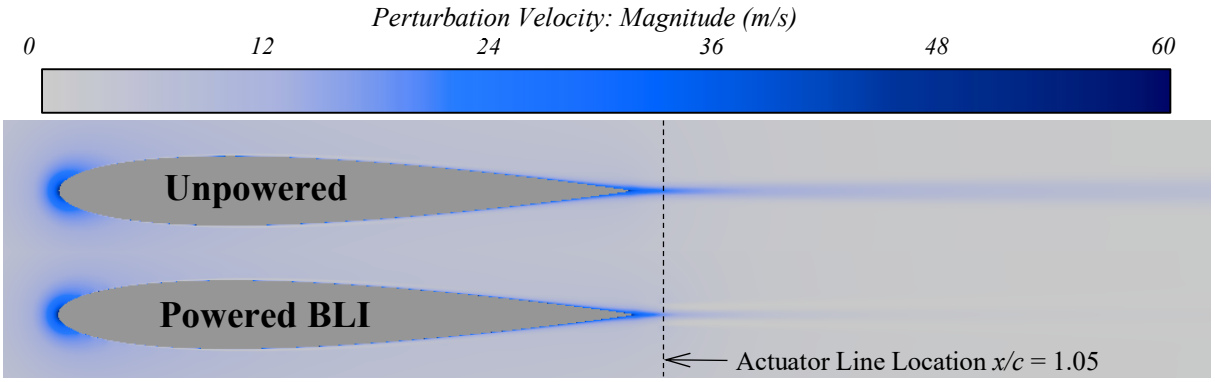

Figure 6 Perturbation Velocity magnitude comparison of the unpowered and powered airfoil

2. Interaction impact on aerodynamic performance: Profile Drag and Surface Dissipation

To assess the integration effects of the airfoil-propulsor assembly on aerodynamic performance, the loss and drag variation coefficients introduced in Section II-A-2 were used. Figure 7 shows that the LVC is relatively invariant to integration effects caused by pressure field interaction of closely coupled bodies compared to the DVC. The LVC yields a consistent profile mechanical energy loss of approximately 3%, attributed to the decrease in wake dissipation

due to attenuation. This behavior highlights an advantage of energy-based methods over *conventional* momentum-based methods for performance assessment of closely coupled bodies, as they are significantly less affected by local changes in pressure gradients.

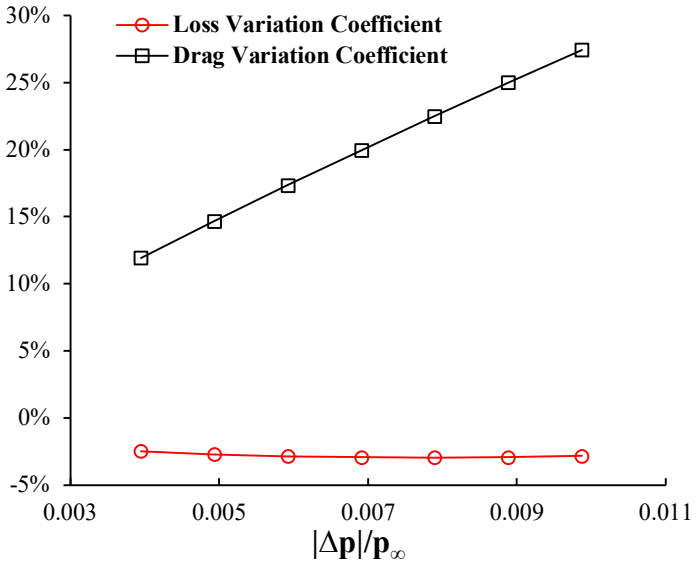

Figure 7 NACA 0012 configuration: LVC and DVC as a function of normalized pressure jump ($|\Delta p|/p_\infty$)

3. *Boundary-Layer Ingestion Performance Assessment: Propulsor Mechanical Energy Inflow & Configuration Net Assembly Force*

The potential power savings obtainable through the propulsor integration at cruise condition were also considered. The cruise condition describes an instance where the configuration is in equilibrium with no deficit or excess in net streamwise force (i.e., $CF_x = 0$). To obtain the power saving coefficient (PSC), the BLI power coefficient (CP_K) was taken at a $CF_x = 0$ via interpolation from the $CP_K(CF_x)$ curves obtained by varying the pressure jump across the AD. The power obtained was then compared against the baseline non-BLI variant to compute the PSC. As a note, the studies presented herein provide PSCs based on comparing configurations with propulsors having similar intake dimensions.

Figure 8 shows the $CP_K(CF_x)$ curves for the baseline, BLI, and unpowered net streamwise force result obtained in [32]. This result was included to confirm the baseline configuration trend, which, when extrapolated to $CP_K = 0$, would coincide with the unpowered net streamwise force.

The BLICs studied were designed by varying the propulsor horizontal ($x' = x/c$) and vertical ($y' = y/c$) positions, which was done to investigate the effects of propulsor positioning on power savings and identify a suitable location for

maximal power benefit. Figure 8(a) shows the net streamwise force coefficient (CF_x) as a function of the power coefficient (CP_K). The results show that by tightly integrating the propulsor with the airframe, namely when the propulsor was centered along the body's longitudinal axis and nearest to the trailing edge, i.e., $x' = 1.01$ and $y' = 0$), 11% less power was required for *cruise* flight, as indicated in the zoomed-in view in Figure 8(b).

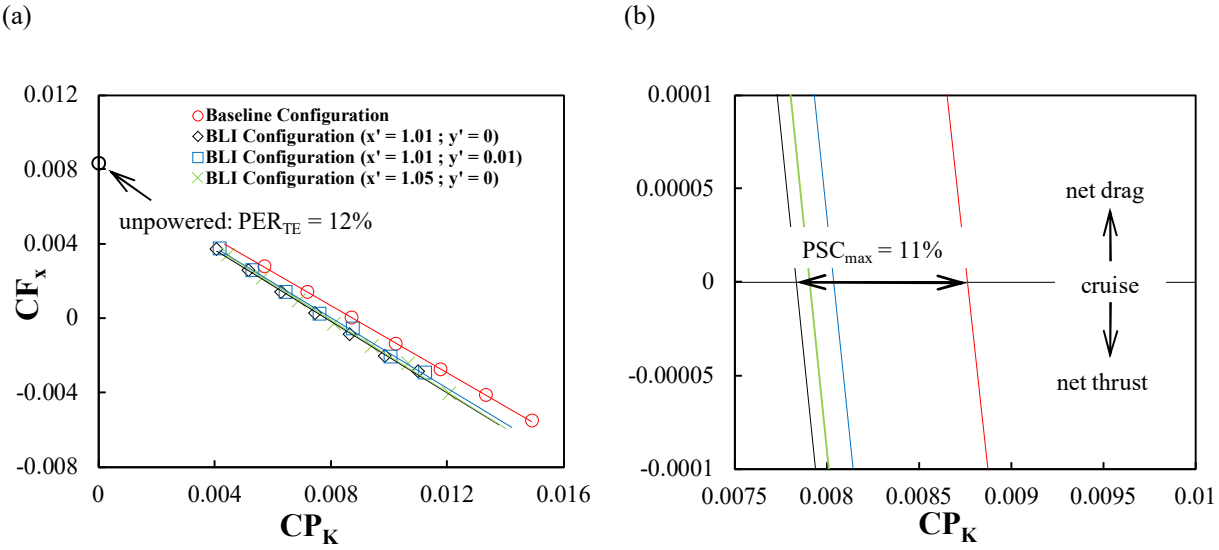

Figure 8 NACA 0012 Airfoil (a) Net streamwise force coefficient vs mechanical flow power coefficient (b) zoomed-in mechanical flow power coefficient at cruise condition

4. Boundary-Layer Ingestion Performance Assessment: Wake Energy Assessment

Using energy methods allows for the integration effects to be assessed from a wake energy perspective. The analyses in this section collectively consider climb, descent, and cruise in steady flight conditions. For descending flight, the potential energy height (CWΓ) component of the PBM becomes a power source. This results in a large amount of wake mechanical energy ($\dot{\varepsilon}_{wake}$) deposition into the downstream wake giving a high E_nWC contribution, as shown in Figure 9(a). This is counterbalanced, both in the decoupled and integrated scenarios, by the jet mechanical energy ($\dot{\varepsilon}_{jet}$) reaching an inflexion point near cruise. Afterward, during climb, the higher propulsive power, or equivalently higher P_K as shown in Figures 9(c) and (d), results in excess jet mechanical energy, increasing the mechanical energy deposition downstream of the trailing edge and raising the E_nWC.

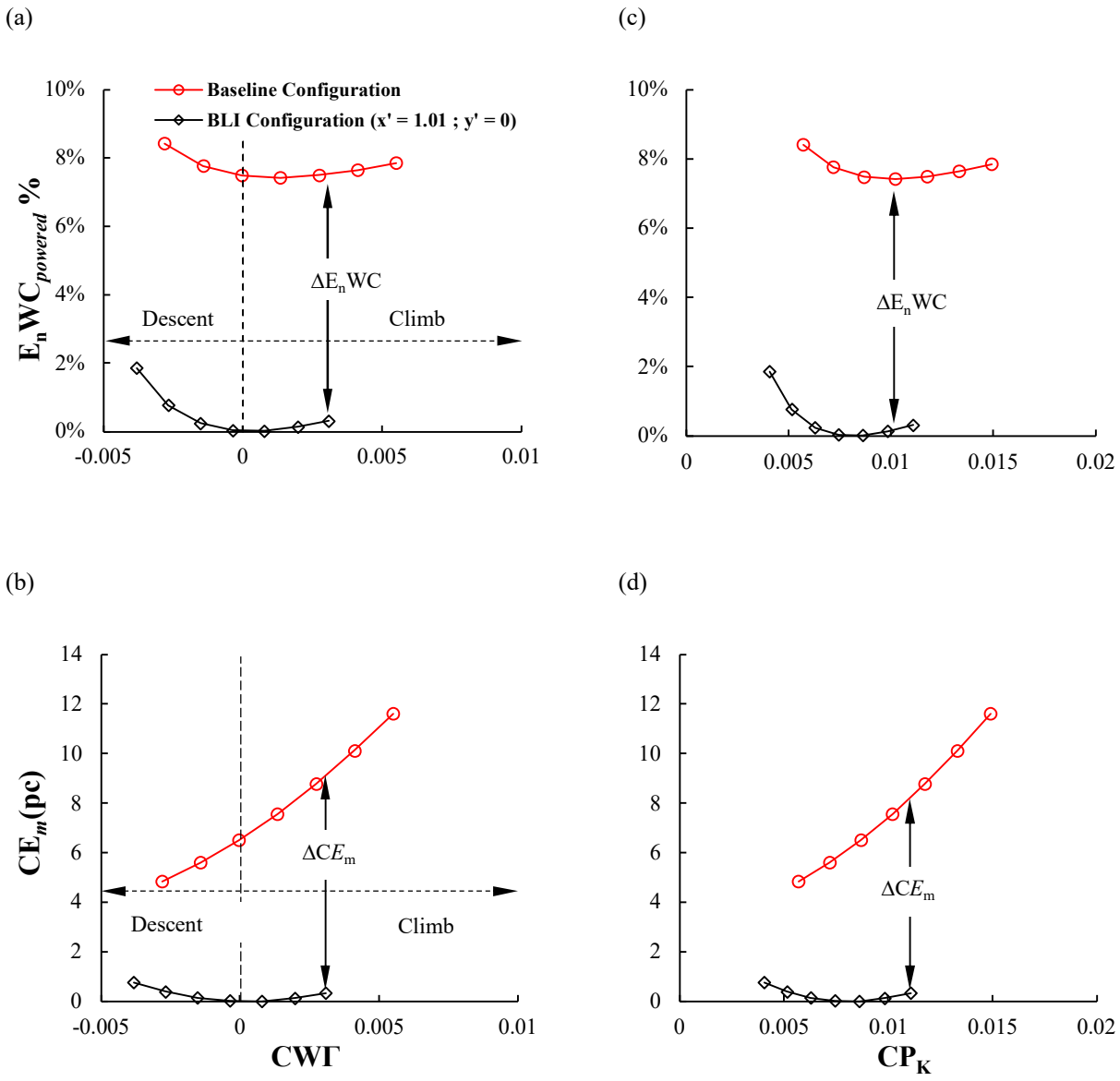

Figure 9 Comparison of BLI and non-BLI configuration E_nWC and CE_m as a function of CWΓ (a & b) and CP_K (c & d) for a BLI NACA 0012 Airfoil

Figure 9(b) shows a noticeable decrease in the wake energy deposition ($\Delta CE_{m,\,cruise} \approx 6.5$ pc[5]), and this trend extends throughout from descending to climbing flight, indicating the benefits of BLICs. In addition to this, an appreciable decrease in the E_nWC was also observed (≈ 7.5%), as shown in Figure 9(c), wherein at this point, the mechanical energy perturbations were attenuated and brought closer to the freestream, decreasing the accumulation of viscous dissipation downstream within the wake.

[5] pc represents power counts for the non-dimesional mechanical energy, i.e. ($CE_m \times 10^{-4}$)

C.Myring Low Drag Body Powered Configuration Analysis

5. *Validation of the Power Balance Formulation for an axisymmetric modeled body of revolution: Myring Low Drag Body configuration*

The unpowered MLDB was coupled with an AD of diameter 0.00305m($d/L_M \approx 0.04\%$) at $x/L_M = 1.01$ and a pressure jump (ΔP) of 57.5 Pa across its interface. For this, a net streamwise force coefficient of $CF_x = -4.11\times10^{-3}$ was observed, resulting in the wake-filling effect shown in Figure 10.

As seen before, the integrated body's downstream wake propagation distance was reduced due to the decrease in wake energy deposition from the attenuated flow.

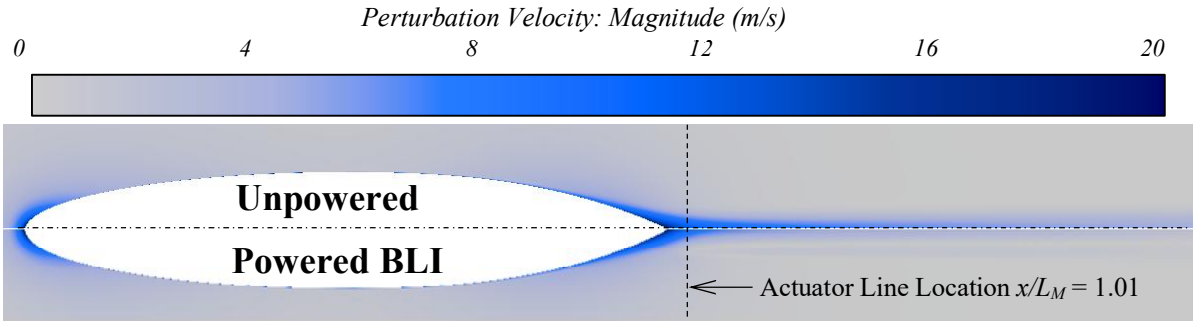

Figure 10 Perturbation Velocity magnitude comparison of the unpowered and powered Myring Low Drag Body

The propulsor power coefficient (CP_Φ) was obtained using the PBM and verified by comparison against the propulsor net mechanical energy flow rate (CP_K), as done prior. The PBM solution in Table 3 showed good agreement, yielding a solution well within $\pm1\%$ of CP_K.

Table 3 Myring Low Drag Body Wake Energy Analysis: Mechanical Energy flow rate and Power Balance solutions

Net streamwise Force	*Net Propulsor Mechanical Energy Flow Rate*	*Power Balance*	
CF_x	CP_K	CP_Φ	$\lvert CP_\Phi - CP_K \rvert / (\%\Delta)$
-4.11×10^{-3}	1.58×10^{-2}	1.60×10^{-2}	1.77×10^{-4} (1.11%)

Similar to the NACA 0012 case study, Figure 11 shows a decrease in wake energy compared to the UC for the streamwise and transverse kinetic energy and the pressure-boundary work rates. This is attributed to the propulsor wake attenuation, which reduces the intensity of the wake-related mechanical energy perturbations while producing thrust.

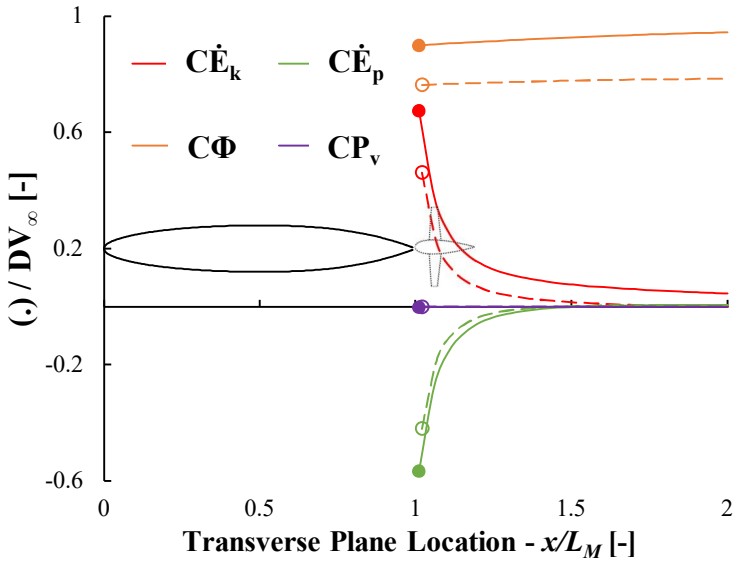

Figure 11 Energy loss rate and dissipation components as a function of Transverse Plane location for the unpowered (− solid) and BLI (− − dashed) Myring Low Drag Body

The aerodynamic performance of the MLDB was also analyzed using the loss- and drag variation coefficients as done prior, shown in Figure 12. The drag variation coefficient was seen again to strongly depend on the pressure gradient, showing a linear increase with the normalized pressure jump. As expected, the loss variation coefficient showed less sensitivity to the propulsor operating condition, showing an approximate 1% decrease in profile mechanical energy losses due to the airframe-propulsor coupling.

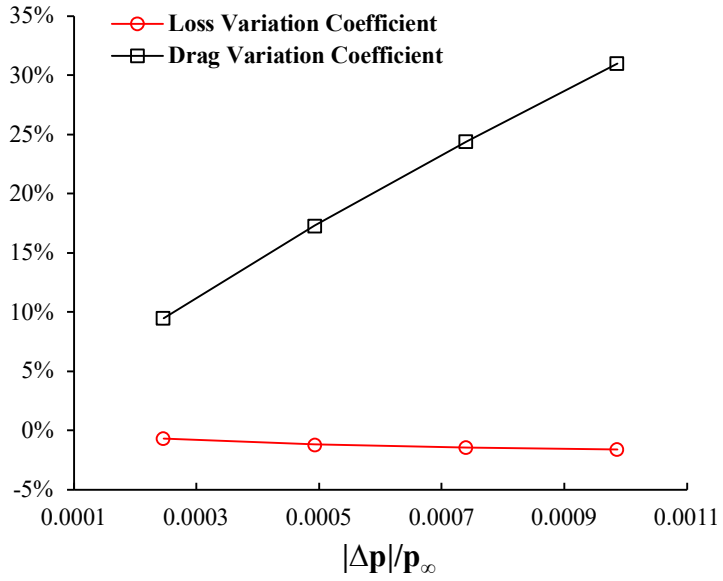

Figure 12 Myring Low Drag Body: LVC and DVC as a function of normalized pressure jump ($|\Delta p|/p_\infty$)

6. Boundary-Layer Ingestion Analysis Near Cruise

Figure 13 shows the $CP_K(CF_x)$ curves for the baseline and BLIC. The unpowered net streamwise force is also indicated, as done in the NACA 0012 analysis. This was seen to agree with the linear trend of the baseline configuration $CP_K(CF_x)$ curve, increasing confidence in the reliability of the obtained solutions. At the simulated cruise condition, a power-saving of ≈4% for the BLI configuration was observed compared to the baseline FIC.

(a) (b)

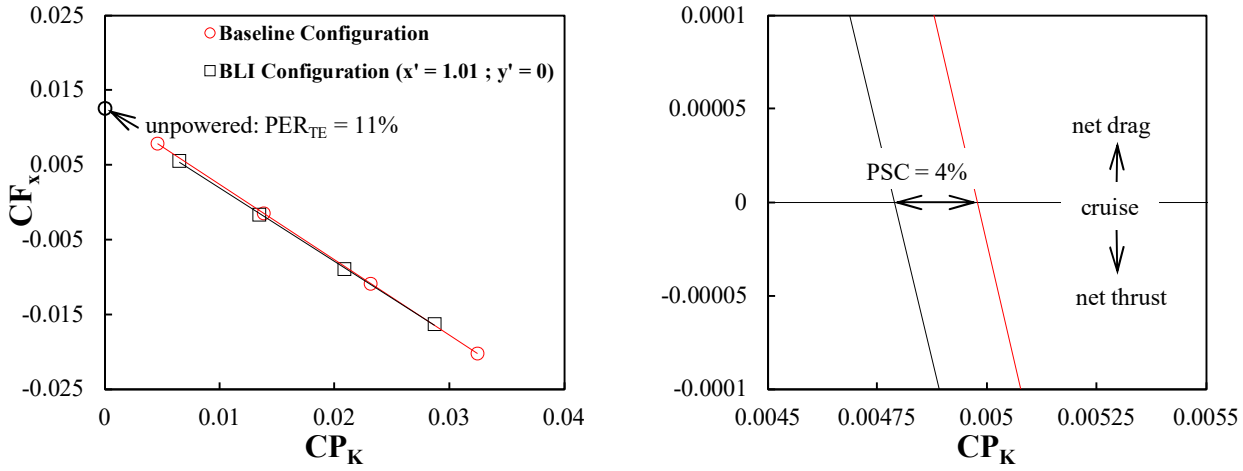

Figure 13 Myring Low Drag Body (a) Net streamwise force coefficient vs. mechanical flow power coefficient (b) zoomed-in mechanical flow power coefficient at cruise condition

7. Boundary-Layer Ingestion Performance Assessment: Mechanical Energy Outflow Rate & Energy Waste Coefficient

The wake energy performance assessment in Figure 14 showed similar trends to those observed in the prior NACA 0012 study, with a decrease in mechanical energy deposition and E_nWC being observed for the BLIC. At cruise, the BLIC was seen to have a reduction in wake mechanical energy deposition (ΔCE_m) of up to ≈5pc with a corresponding ≈4% decrease in E_nWC compared to the baseline.

Figures 14(a) and (c) also show a crossover between the baseline and BLIC if extrapolated to higher climb rates. This implies that at higher propulsive power demands, the baseline configuration performs better in terms of how efficiently it utilizes its available energy content to produce propulsive force. This is because of the inadvertent constraint imposed on the mass flow rate, as each configuration has propulsors with the same dimensions. This entails a lower mass flow for the BLIP, which does not pose a problem for flight conditions near cruise as the BLI benefit outweighs the effect of the mass flow deficit. In this instance, the BLI benefit refers mainly to the decrease in jet velocity when producing propulsive force.

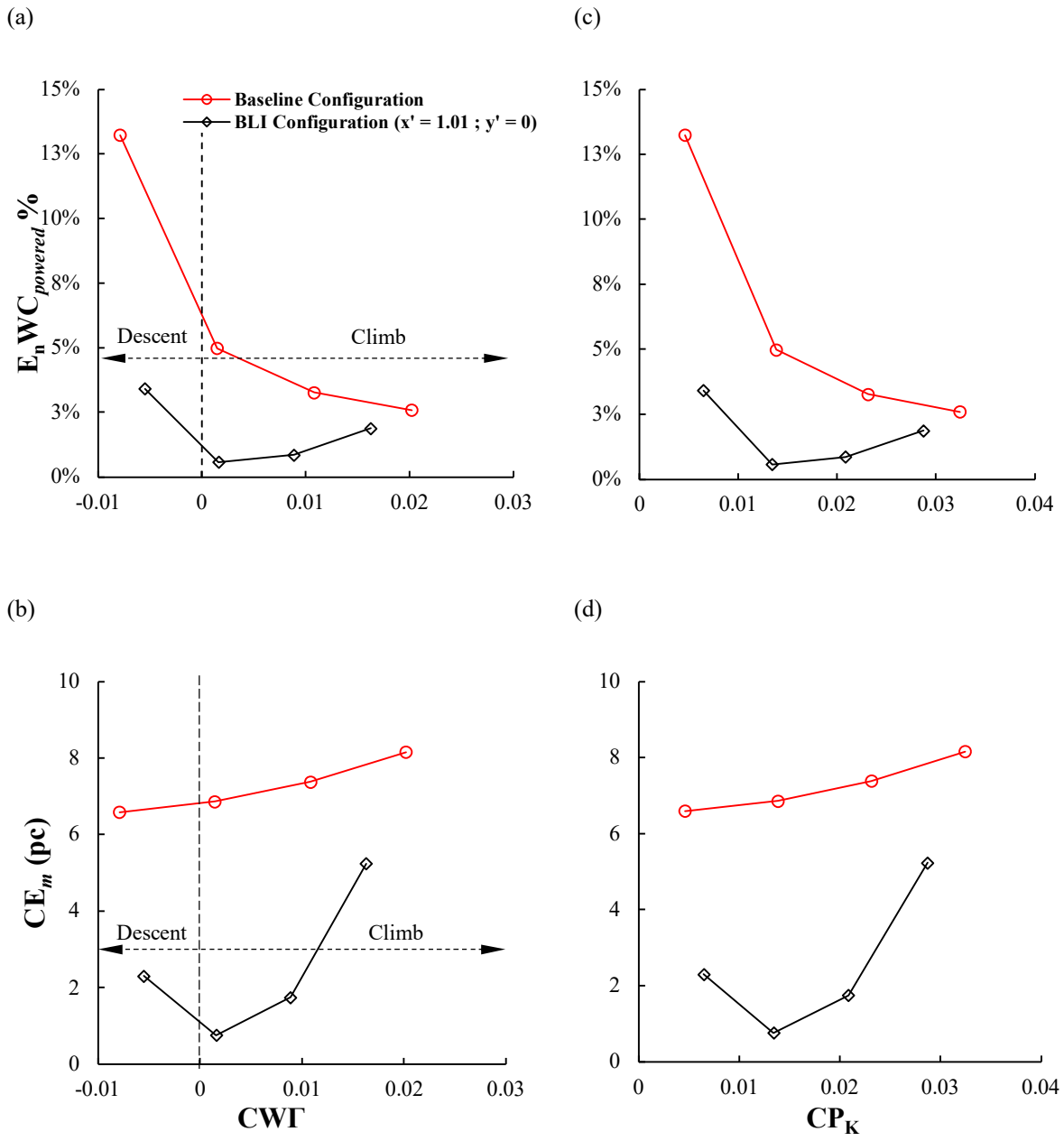

Figure 14 Comparison of BLI and non-BLI configuration E_nWC and CE_m as a function of CWΓ (a & b) and CP_K (c & d) for a BLI Myring Low Drag Body

At high propulsive power demands, the BLIP supplements the deficit in mass flow by increasing the jet velocity to meet the thrust requirement, which increases the mechanical energy deposition and E_nWC. The crossover mentioned earlier occurs when the effects of the mass flow deficit overshadow the BLI benefit.

Additionally, Figures 14(b) and (d) show that the baseline configuration has a much slower rate of change in CE_m with increasing propulsive power demand compared to the BLIC. This occurs due to the constant pressure jump across the

AD. For BLICs, this results in particular regions downstream of the AD having a significant momentum excess which is less favorable as it contributes to the mechanical energy losses.

D.F-57 Low Drag Body Powered Configuration Analysis

8. Validation of the Power Balance Formulation for a three-dimensionally modeled body of revolution: F-57 Low Drag Body configuration

The final investigation focuses on the powered F-57 Low Drag Body, wherein the effects of the amount of boundary layer ingested and the method through which momentum is imparted were briefly assessed. This was done by sizing the AD to be noticeably larger than the boundary layer height. The AD diameter was 0.025m (d/LF ≈ 2%) at x/L_F = 1.0 with a pressure jump (ΔP) of 15Pa across its actuator interface. This gave a net streamwise force coefficient of $CF_x = -2.04\times10^{-2}$ yielding the wake-filling characteristics illustrated in Figure 15.

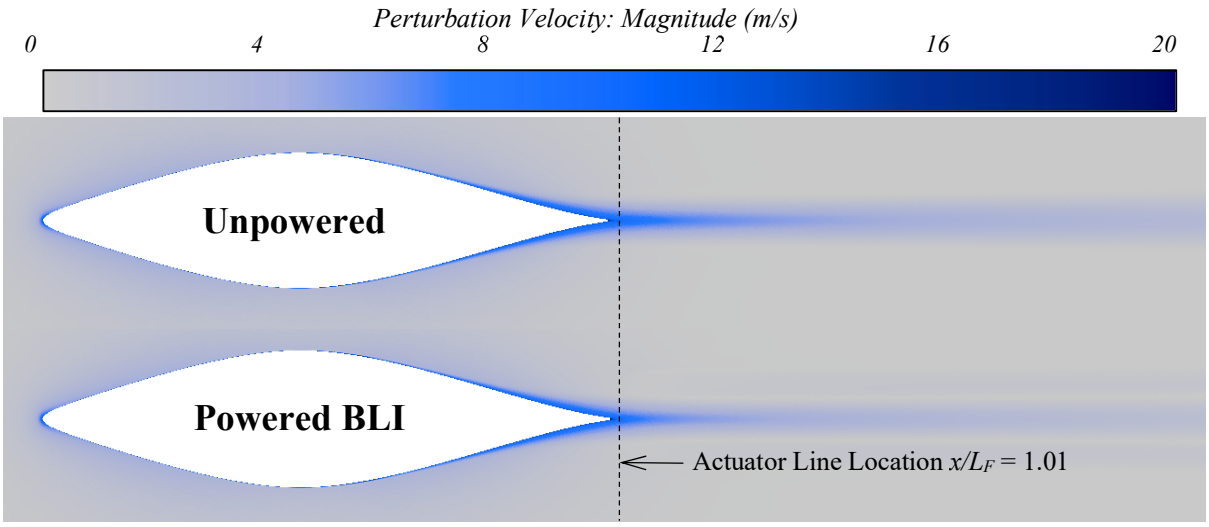

Figure 15 Perturbation Velocity magnitude comparison of the unpowered and powered F-57 Low Drag Body

The power coefficient comparison between the net propulsor mechanical energy flow rate (CP_K) and the PBM (CP_Φ) in Table 4 showed a < 1% difference between their solutions. The close agreement between these values highlights the reliability of the PBM for powered flows, as the power inflow from the propulsor can be evaluated directly from CP_K or indirectly through a summation of the PBM outflow terms represented as CP_Φ.

Table 4 F-57 Low Drag Body Wake Energy Analysis: Mechanical Energy flow rate and Power Balance solutions

Net streamwise Force	*Net Propulsor Mechanical Energy Flow Rate*	*Power Balance*	
CF_x	CP_K	CP_Φ	$\lvert CP_\Phi - CP_K \rvert / (\%\Delta)$
-2.04×10^{-2}	1.52×10^{-2}	1.53×10^{-2}	9.66×10^{-5} (0.63%)

As with the NACA 0012 and MLDB cases, the reduced energy loss via BLI decreased the downstream wake propagation distance, as shown in Figure 15. This effect is also evident in Figure 16, through the decrease in wake mechanical energy imparted to the flow due to the more efficient utilization of the available energy compared to the freestream ingesting propulsor (FIP).

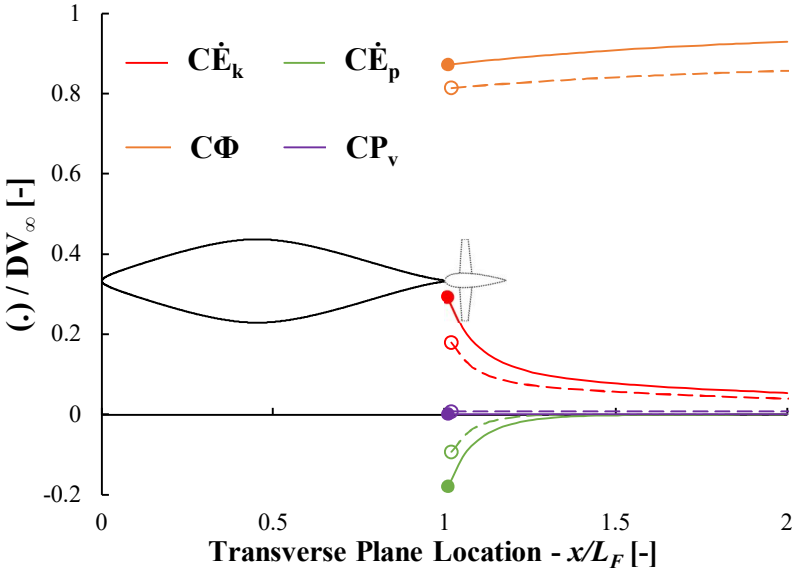

Figure 16 Energy loss rate and dissipation components as a function of Transverse Plane location for the unpowered (− solid) and BLI (− − dashed) F-57 Low Drag Body

The loss and drag variation coefficients are compared in Figure 17, where the loss variation coefficient indicated a performance improvement with a 1% decrease in profile mechanical energy losses due to the airframe-propulsor coupling.

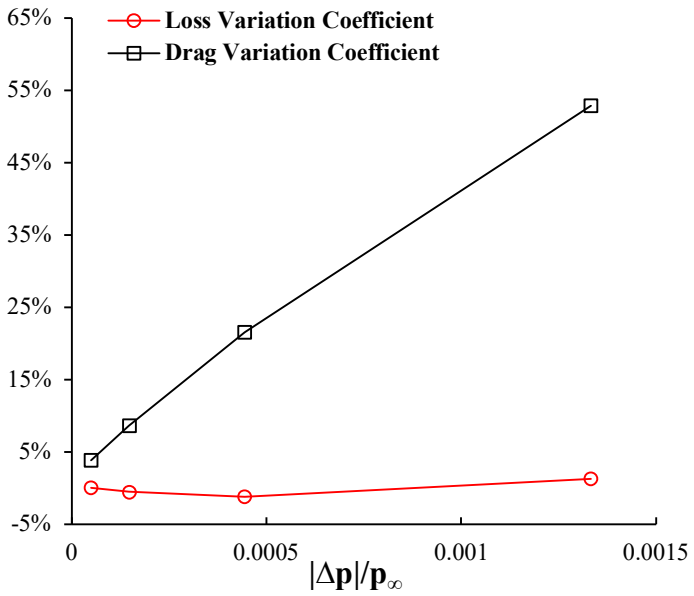

Figure 17 F-57 Low Drag Body: LVC and DVC as a function of normalized pressure jump ($|\Delta p|/p_\infty$)

9. Boundary-Layer Ingestion Benefit near Cruise

The powered baseline and BLIC $CP_K(CF_x)$ curves are plotted in Figure 18(a), with a zoomed-in representation in Figure 18(b) highlighting the cruise operating point. The UC net streamwise force intuitively agreed with the trend obtained for the baseline FIC when extrapolated to a power-off condition (i.e., $P_K = 0$). At cruise, Figures 18(b) and (d) show that the BLIC requires 5% less power for cruising flight compared to the FIC.

(a) (b)

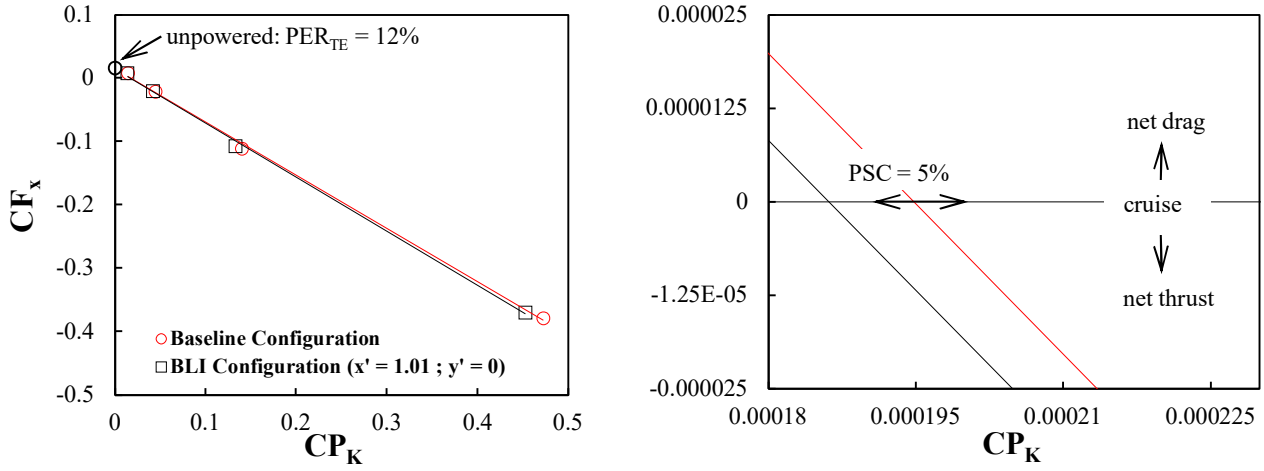

Figure 18 F-57 Low Drag Body (a) Net streamwise force coefficient vs mechanical flow power coefficient (b) zoomed-in mechanical flow power coefficient at cruise condition

10. Boundary-Layer Ingestion Performance Assessment: Energy Waste Coefficient

The wake energy assessment confirms that BLIPs reduce the waste of mechanical energy within the wake through attenuation, evidenced by the offset in E_nWC and CE_m shown in Figure 19. However, the extent of this benefit, viewed through ΔE_nWC or ΔCE_m, is significantly reduced. This comes from the inefficient way the propulsor imparts momentum to the flow, which is done through a uniform distribution across the propulsor interface, as highlighted before in the MLDB study.

As the BLIP size is much larger relative to the size of the boundary layer, this broadens the regions of influence wherein momentum is in excess. This raises the amount of wasted mechanical energy downstream, indicated by the increased magnitude of CE_m in Figures 19(b) and (d), thus reducing the BLI benefit.

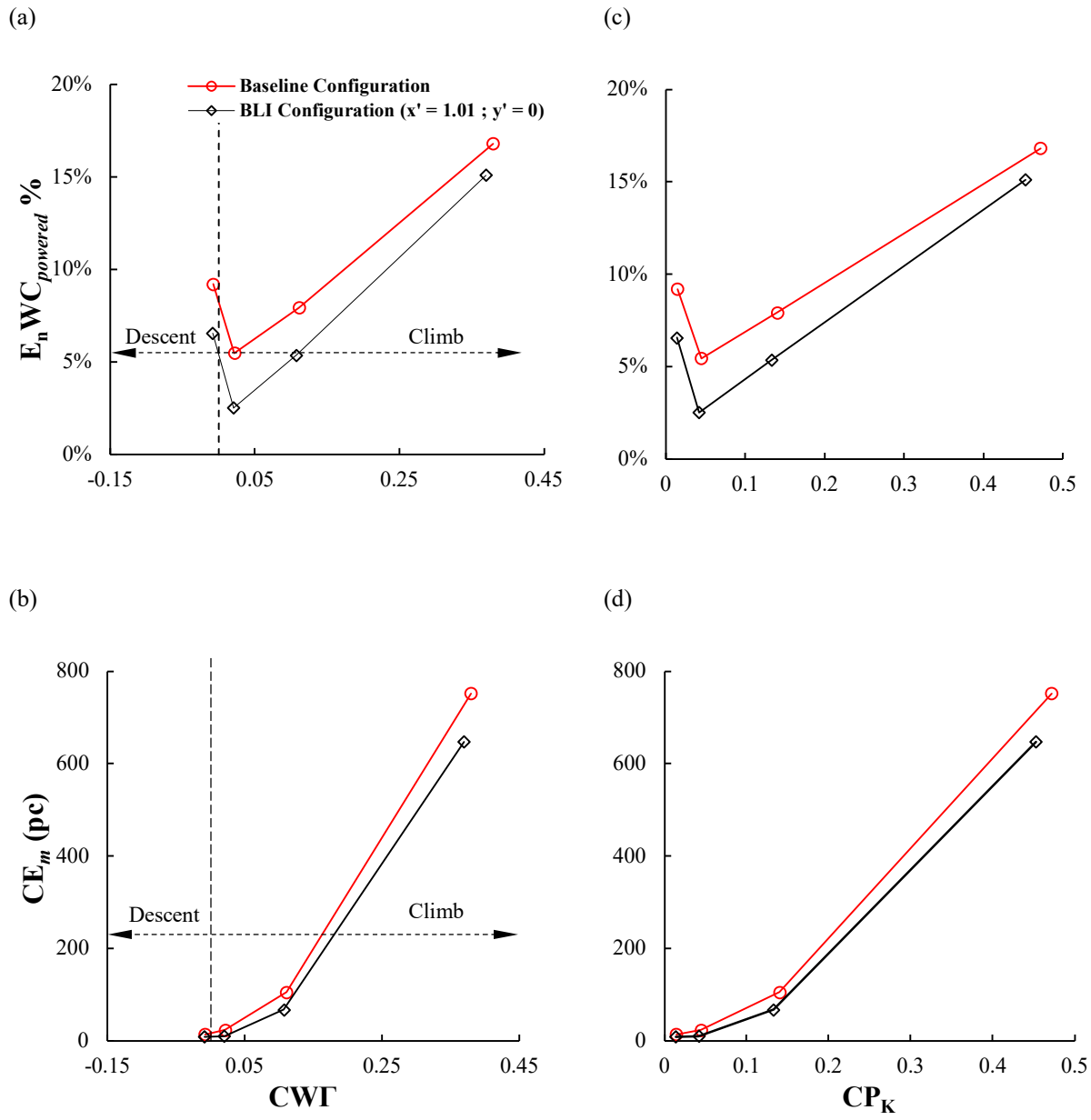

Figure 19 Comparison of BLI and non-BLI configuration E_nWC and CE_m as a function of CWΓ (a & b) and CP_K (c & d) for a BLI F-57 Low Drag Body

IV. Discussion of Results

The aerodynamic performance of each study was verified through a mechanical energy analysis of the balance in powers (i.e., power-in and outflow). Good agreement was seen in each study with a < 1% difference between the alternative evaluations, thus verifying the applicability of PBM analyses. These solutions were later fed into the PSC evaluation based on the formulation provided by Blumenthal et al. [33–35].

Performance analysis through the PSC allows for a comparative assessment of the benefits observed between BLIC and FIC. However, in as much as this is true, it is essential to note the nuanced complexities of this factor which arise from its subjectivity to the characteristics of the reference FIC chosen for comparison. Hall et al. [28] illustrate that the PSC is not unique but dependent on the choice and type of BLIP design, each carrying inherent limitations imposed by either intentional or inadvertent constraints.

PSC analyses may entail a comparison of designs matching either one or a combination of the following properties:

i. Mechanical flow power (P_K)

ii. Propulsive efficiency

iii. Jet velocity

iv. Jet area

v. Propulsor mass flow

This list is not exhaustive but aids in highlighting the various considerations and forms through which comparative analyses between BLIPs and FIPs may be conducted. Based on the chosen matching of design parameters between the boundary layer and freestream ingesting configurations, the extent and interpretation of the origin of power saving and BLI benefit tend to change. The work conducted in this research uses AD propulsors with the same dimensions (category iv) between the boundary layer and freestream ingesting configurations, immediately constraining the propulsor BLIP mass flow. This effect became particularly evident at high propulsive power demands, particularly during climb. Figure 14 shows this limit where the impact of the BLIP mass flow deficit outweighs its BLI benefit. In this instance, the mass flow deficit of the BLIP is supplemented by increasing the jet velocity, which raises the mechanical energy deposition downstream.

The studies conducted showed that BLI benefits could be observed in a variety of ways, such as a reduction in the mechanical energy inflow (P_K) necessary to produce propulsive force, as shown through the PSC in Figures 8, 13, and 18, a decrease in the profile mechanical energy loss shown through the LVC in Figures 7, 12 and 17, or a reduction in the mechanical energy deposition shown through $\Delta E_n WC$ and ΔCE_m in Figures 9, 14 and 19.

Performance assessment was also conducted using the momentum-based DVC, which indicated an apparent "detriment" due to BLI integration, as shown in the summary in Figure 20. This observation is not representative of

the actual performance of the configuration as this metric is not well suited for analyzing HICs where pressure-field interference effects are prevalent.

As a result, it is recommended that energy or exergy-based analysis be used for the performance assessment of such configurations. These methods provide a comprehensive decomposition of aerodynamic force into phenomenological contributions and are less influenced by interference effects caused by local changes in pressure gradients, making them more suitable for analyzing closely coupled bodies.

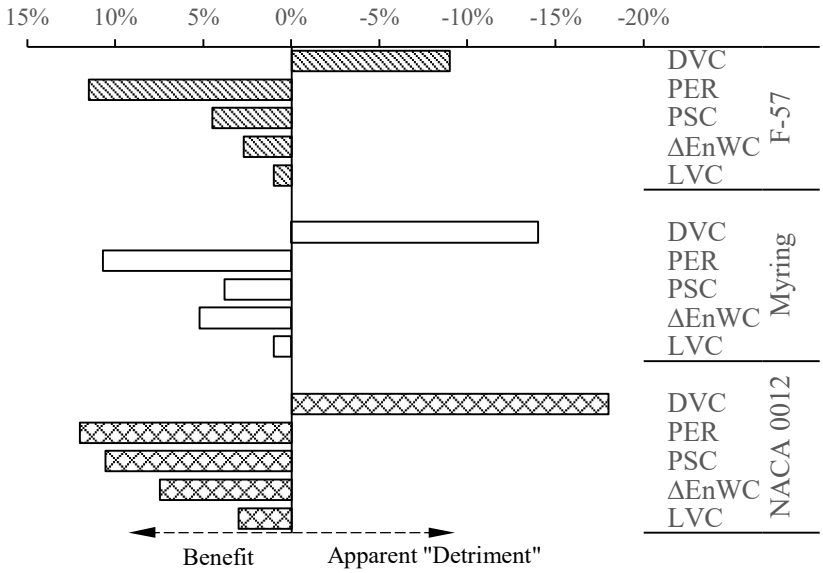

Figure 20 Boundary layer ingestion configurations cruise case study results summary

A particular area warranting further investigation is the relation between PER and PSC, the derivation provided in the Appendix highlights the strong dependence of PSC on the BLIP's wake attenuation and propulsive efficiencies. Through this, it is possible to show that a maximum PSC at cruise (i.e., PER) is approached when both these efficiencies approach unity. With this in mind, it is possible to gauge the efficacy of a BLIP through an assessment of E_nWC as well as the relative difference in magnitude between PER and PSC.

The studies showed that the NACA 0012 BLIP outperformed the other candidates, offering the highest PSC and decreased E_nWC owing to its good wake attenuation characteristics. The decrease in the BLIP efficacy for the BoR (i.e., MLDB and F-57) was attributed to the method of momentum addition via the propulsor. The AD imparted a constant pressure jump across its interface, which resulted in a significant momentum excess in certain regions, contributing toward an increased E_nWC and CE_m.

V. Conclusions

The work herein focuses on the aerodynamic assessment of planar and axisymmetric bodies employing boundary layer ingestion. The case studies included a NACA 0012 airfoil as well as the Myring and F-57 Low drag bodies coupled with AD propulsor models with a constant pressure jump specified across their interfaces. The propulsor model was verified by comparing its thrust, power, and propulsive efficiency using actuator disk and power balance methods, with all solutions showing an overall good agreement between their respective results.

After verification, the case studies evaluated the relative BLI benefit for the various bodies compared to traditional freestream ingesting variants. An observed advantage of ingesting boundary layer flow was shown through decreased power consumption to produce propulsive force assessed through the PSC. The LVC and E_nWC metrics were also used for assessment, which compared the profile mechanical energy loss (i.e., wake and surface dissipation) and the mechanical energy deposition in the downstream wake, respectively. For the BLICs, wake attenuation due to the propulsor resulted in less mechanical energy deposition and accumulation of dissipation downstream. Using these metrics, the BLIPs showed a clear decrease in power demand via a positive PSC. This, however, was limited to conditions where this benefit was not outweighed by the effect of the incurred mass flow deficit due to the ingestion of the boundary layer instead of freestream flow. In this instance, the BLIP would compensate for the deficit by increasing the jet velocity, thus increasing the downstream energy deposition and associated dissipation.

Lastly, the discussion on the relationship between PER and PSC helped highlight the dependence of the performance benefits on the propulsive as well as wake attenuation efficiencies of the BLIP. Through this, it is possible to observe that the benefits reported in the case studies can be improved by using distributed wake-attenuating ADs instead of the uniform model chosen. This would better the BLIP wake attenuation efficiency improving the method through which momentum is imparted to the flow to produce propulsive force.

Appendix: Energy Recovery Potential Relationship with Power saving Coefficient

This section aims to illustrate the significance of PER and its implications on powered BLI analyses. To achieve this, we start with the general formulation of PSC provided in equation (2). It can be observed that the net propulsor mechanical energy inflow can be related to the total mechanical energy loss. This can be split into various physical mechanisms such as surface, wake, and jet losses (see equation (15)).

$$PSC = 1 - \frac{P_K}{P'_K} = 1 - \frac{\Phi^*}{\Phi'^*} = 1 - \frac{\Phi_{surf} + \Phi^*_{wake} + \Phi^*_{jet}}{\Phi'_{surf} + \Phi'^*_{wake} + \Phi'^*_{jet}} \tag{15}$$

Observing the behavior when the propulsive efficiencies of the BLI and FIPs approach unity yields the PSC expression described in equation (16). Furthermore, taking the limit when the attenuation efficiency approaches unity shows that the PSC becomes equal to the maximum PER for the UC, i.e., PER_{TE}.

$$\begin{aligned} &\lim_{(\eta'_{prop}, \eta_{prop}) \to 1} PSC|_{F_x = 0} = 1 - \frac{\Phi_{surf} + \Phi^*_{wake}}{\underbrace{\Phi'_{surf} + \Phi'^*_{wake}}_{\Phi'_p = \boldsymbol{F}_B \cdot \boldsymbol{V}_\infty}} \\ &= \underbrace{1 - \frac{\Phi_{surf}}{\boldsymbol{F}_B \cdot \boldsymbol{V}_\infty}}_{PER_{TE}} - \frac{\Phi^*_{wake}}{\boldsymbol{F}_B \cdot \boldsymbol{V}_\infty} \text{ assuming } \Phi_{surf} = \Phi'_{surf} \end{aligned} \tag{16}$$

This implies that under the assumptions mentioned, the PER provides a theoretical maximum of attainable benefits with BLI/wake attenuating propulsors, wherein the PSC benefits approach this value when the propulsive and wake attenuating efficiencies of the BLIP approach unity (see equation (17)).

$$\begin{aligned} &\text{since } \lim_{\eta_{att.} \to 1} \frac{\Phi^*_{wake}}{\boldsymbol{F}_B \cdot \boldsymbol{V}_\infty} = 0 \\ &\therefore \lim_{\eta_{att.} \to 1} PSC|_{F_x = 0} = PER_{TE} \end{aligned} \tag{17}$$

Acknowledgments

The authors would like to thank the University of Pretoria Department of Research and Innovation as well as Cranfield School of Aerospace, Transport, and Manufacturing for their support and funding during the development of this work. The authors would also like to thank Nicolas G. M. Moirou and Ioannis Lamprakis for their insight and advice toward the outcomes of this work.

References

[1] Welstead, J., and Felder, J. L., "Conceptual Design of a Single-Aisle Turboelectric Commercial Transport with Fuselage Boundary Layer Ingestion," *54th AIAA Aerospace Sciences Meeting*, 2016. https://doi.org/10.2514/6.2016-1027

[2] Isikveren, A. T., Seitz, A., Bijewitz, J., Mirzoyan, A., Isyanov, A., Grenon, R., Atinault, O., Godard, J. L., and Stückl, S., "Distributed Propulsion and Ultra-High by-Pass Rotor Study at Aircraft Level," *Aeronautical Journal*, Vol. 119, No. 1221, 2015, pp. 1327–1376. https://doi.org/10.1017/S0001924000011295

[3] Seitz, A., Bijewitz, J., Kaiser, S., and Wortmann, G., "Conceptual Investigation of a Propulsive Fuselage Aircraft Layout," *Aircraft Engineering and Aerospace Technology*, Vol. 86, No. 6, 2014, pp. 464–472. https://doi.org/10.1108/AEAT-06-2014-0079

[4] Uranga, A., Drela, M., Hall, D. K., and Greitzer, E. M., "Analysis of the Aerodynamic Benefit from Boundary Layer Ingestion for Transport Aircraft," *AIAA Journal*, Vol. 56, No. 11, 2018, pp. 4271–4281. https://doi.org/10.2514/1.J056781

[5] Drela, M., "Development of the D8 Transport Configuration," *29th AIAA Applied Aerodynamics Conference*, 2011. https://doi.org/10.2514/6.2011-3970

[6] Uranga, A., Drela, M., Greitzer, E., Titchener, N., Lieu, M., Siu, N., Huang, A., Gatlin, G. M., and Hannon, J., "Preliminary Experimental Assessment of the Boundary Layer Ingestion Benefit for the D8 Aircraft," *52nd Aerospace Sciences Meeting*, 2014. https://doi.org/10.2514/6.2014-0906

[7] Pandya, S. A., Uranga, A., Espitia, A., and Huang, A., "Computational Assessment of the Boundary Layer Ingesting Nacelle Design of the D8 Aircraft," *52nd Aerospace Sciences Meeting*, 2014. https://doi.org/10.2514/6.2014-0907

[8] Uranga, A., Drela, M., Greitzer, E. M., Hall, D. K., Titchener, N. A., Lieu, M. K., Siu, N. M., Casses, C., Huang, A. C., Gatlin, G. M., and Hannon, J. A., "Boundary Layer Ingestion Benefit of the D8 Transport Aircraft," *AIAA Journal*, Vol. 55, No. 11, 2017, pp. 3693–3708. https://doi.org/10.2514/1.J055755

[9] Marien, T. V., Welstead, J. R., and Jones, S. M., "Vehicle-Level System Impact of Boundary Layer Ingestion for the NASA D8 Concept Aircraft," *AIAA Aerospace Sciences Meeting*, 2018. https://doi.org/10.2514/6.2018-0271

[10] Wiart, L., Atinault, O., Grenon, R., Paluch, B., and Hue, D., "Development of NOVA Aircraft Configurations for Large Engine Integration Studies," *33rd AIAA Applied Aerodynamics Conference*, 2015. https://doi.org/10.2514/6.2015-2254

[11] Wiart, L., Atinault, O., Boniface, J. C., and Barrier, R., "Aeropropulsive Performance Analysis of the NOVA Configurations," *30th Congress of the International Council of the Aeronautical Sciences, ICAS*. Daejeon, Korea, 2016, pp. 1–11.

[12] Romani, G., Ye, Q., Avallone, F., Ragni, D., and Casalino, D., "Numerical Analysis of Fan Noise for the NOVA Boundary-Layer Ingestion Configuration," *Aerospace Science and Technology*, Vol. 96, 2020, p. 105532. https://doi.org/10.1016/j.ast.2019.105532

[13] Valencia, E., Hidalgo, V., Nalianda, D., Laskaridis, P., and Singh, R., "Discretized Miller Approach to Assess Effects on Boundary Layer Ingestion Induced Distortion," *Chinese Journal of Aeronautics*, Vol. 30, No. 1, 2017, pp. 235–248. https://doi.org/10.1016/j.cja.2016.12.005

[14] Felder, J., Kim, H., and Brown, G., "Turboelectric Distributed Propulsion Engine Cycle Analysis for Hybrid-Wing-Body Aircraft," *47th AIAA Aerospace Sciences Meeting including The New Horizons Forum and Aerospace Exposition*, 2009. https://doi.org/10.2514/6.2009-1132

[15] Laskaridis, P., "Assessment of Distributed Propulsion Systems Used with Different Aircraft Configurations," *51st AIAA/SAE/ASEE Joint Propulsion Conference*, 2015. https://doi.org/10.2514/6.2015-4029

[16] Goldberg, C., Nalianda, D., Pilidis, P., and Singh, R., "Performance Assessment of a Boundary Layer Ingesting Distributed Propulsion System at Off-Design," *53rd AIAA/SAE/ASEE Joint Propulsion Conference*, 2017. https://doi.org/10.2514/6.2017-5055

[17] Kim, H., and Liou, M. F., "Flow Simulation and Drag Decomposition Study of N3-X Hybrid Wing-Body Configuration," *Aerospace Science and Technology*, Vol. 85, 2019, pp. 24–39. https://doi.org/10.1016/j.ast.2018.11.047

[18] Plas, A., Crichton, D., Sargeant, M., Hynes, T., Greitzer, E., Hall, C., and Madani, V., "Performance of a Boundary Layer Ingesting (BLI) Propulsion System," *45th AIAA Aerospace Sciences Meeting and Exhibit*, 2007. https://doi.org/10.2514/6.2007-450

[19] Arntz, A., and Atinault, O., "Exergy-Based Performance Assessment of a Blended Wing–Body with Boundary-Layer Ingestion," *AIAA Journal*, Vol. 53, No. 12, 2015, pp. 3766–3776. https://doi.org/10.2514/1.J054072

[20] AGARD MIDAP Study Group, "Guide to In-Flight Thrust Measurement of Turbojets and Fan Engines," AGARD-AG-237, 1979.

[21] E-33 In Flight Propulsion Measurement Committee, "In-Flight Thrust Determination," AIR1730A/B, SAE International, 2017.

[22] Sanders, D. S., and Laskaridis, P., "Full-Aircraft Energy-Based Force Decomposition Applied to Boundary-Layer Ingestion," *AIAA Journal*, Vol. 58, No. 10, 2020, pp. 4357–4373. https://doi.org/10.2514/1.J058695

[23] Guha, A., "Optimum Fan Pressure Ratio for Bypass Engines with Separate or Mixed Exhaust Streams," *Journal of Propulsion and Power*, Vol. 17, No. 5, 2001, pp. 1117–1122. https://doi.org/10.2514/2.5852

[24] Guha, A., Boylan, D., and Gallagher, P., "Determination of Optimum Specific Thrust for Civil Aero Gas Turbine Engines: A Multidisciplinary Design Synthesis and Optimisation," *Proceedings of the Institution of Mechanical Engineers, Part G: Journal of Aerospace Engineering*, Vol. 227, No. 3, 2013, pp. 502–527. https://doi.org/10.1177/0954410011435623

[25] Davidson, I. M., "Some Notes on Aircraft Propulsion by Wake Regeneration," *Annals of the New York Academy of Sciences*, Vol. 154, No. 2 International, 1968, pp. 641–651. https://doi.org/10.1111/j.1749-6632.1968.tb15219.x

[26] Thurston, S., and Evanbar, M. S., "Efficiency of a Propulsor on a Body of Revolution-Inducting Boundary-Layer Fluid," *Journal of Aircraft*, Vol. 3, No. 3, 1966, pp. 270–277. https://doi.org/10.2514/3.43737

[27] Betz, A., "Introduction to the Theory of Flow Machines," Pergamon Press, United Kingdom, 1966, pp. 214–218. https://doi.org/10.1016/C2013-0-05426-6

[28] Hall, D. K., Huang, A. C., Uranga, A., Greitzer, E. M., Drela, M., and Sato, S., "Boundary Layer Ingestion Propulsion Benefit for Transport Aircraft," *Journal of Propulsion and Power*, Vol. 33, No. 5, 2017, pp. 1118–1129. https://doi.org/10.2514/1.B36321

[29] Smith, L. H., "Wake Ingestion Propulsion Benefit," *Journal of Propulsion and Power*, Vol. 9, No. 1, 1993, pp. 74–82. https://doi.org/10.2514/3.11487

[30] Drela, M., "Power Balance in Aerodynamic Flows," *AIAA Journal*, Vol. 47, No. 7, 2009, pp. 1761–1771. https://doi.org/10.2514/1.42409

[31] Sato, S., "The Power Balance Method For Aerodynamic Performance Assessment," Ph.D. Dissertation, Massachusetts Institute of Technology, 2012.

[32] Mutangara, N. E., Smith, L., Craig, K. J., and Sanders, D. S., "Potential for Energy Recovery of Unpowered Configurations Using Power Balance Method Computations," *Journal of Aircraft*, Vol. 58, No. 6, 2021, pp. 1364–1374. https://doi.org/10.2514/1.C036172

[33] Blumenthal, B. T., "Computational Investigation of a Boundary-Layer Ingesting Propulsion System for the Common Research Model," MSc Thesis, The Pennsylvania State University, 2016.

[34] Blumenthal, B., Elmiligui, A. A., Geiselhart, K., Campbell, R. L., Maughmer, M. D., and Schmitz, S., "Computational Investigation of a Boundary Layer Ingestion Propulsion System for the Common Research Model," *46th AIAA Fluid Dynamics Conference*, 2016. https://doi.org/10.2514/6.2016-3812

[35] Blumenthal, B. T., Elmiligui, A. A., Geiselhart, K. A., Campbell, R. L., Maughmer, M. D., and Schmitz, S., "Computational Investigation of a Boundary-Layer-Ingestion Propulsion System," *Journal of Aircraft*, Vol. 55, No. 3, 2018, pp. 1141–1153. https://doi.org/10.2514/1.C034454

[36] Baskaran, P., Corte, B. della, van Sluis, M., and Rao, A. G., "Aeropropulsive Performance Analysis of Axisymmetric Fuselage Bodies for Boundary-Layer Ingestion Applications," *AIAA Journal*, Vol. 60, No. 3, 2022, pp. 1592–1611. https://doi.org/10.2514/1.J060362

[37] Arntz, A., and Hue, D., "Exergy-Based Performance Assessment of the NASA Common Research Model," *AIAA Journal*, Vol. 54, No. 1, 2016, pp. 88–100. https://doi.org/10.2514/1.J054127

[38] Arntz, A., "Civil Aircraft Aero-Thermo-Propulsive Performance Assessment by an Exergy Analysis of High-Fidelity CFD-RANS Flow Solutions," Ph.D. Dissertation, Université de Lille, Lille,France, 2014.

[39] Arntz, A., Atinault, O., Destarac, D., and Merlen, A., "Exergy-Based Aircraft Aeropropulsive Performance Assessment: CFD Application to Boundary Layer Ingestion," *32nd AIAA Applied Aerodynamics Conference*, 2014. https://doi.org/10.2514/6.2014-2573

[40] Yildirim, A., Gray, J. S., Mader, C. A., and Martins, J. R. R. A., "Boundary-Layer Ingestion Benefit for the STARC-ABL Concept," *Journal of Aircraft*, Vol. 59, No. 4, 2022, pp. 896–911. https://doi.org/10.2514/1.C036103

[41] Mutangara, N., Smith, L., Craig, P. K. J., and Sanders, D. S., "Numerical Implementation of the Power Balance Method for Aerodynamic Performance Assessment," MSc Thesis, University of Pretoria, 2020.
[42] Jespersen, D. C., Pulliam, T. H., and Childs, M. L., "OVERFLOW Turbulence Modeling Resource Validation Results," NAS Technical Report: NAS-2016-01, 2016.
[43] Myring, D. F., "A Theoretical Study of the Effects of Body Shape and Mach Number on the Drag of Bodies of Revolution in Subcritical Axisymmetric Flow," Farnborough, Hants, UK, 1981.
[44] Patel, V. C., and Lee, Y. T., "Thick Axisymmetric Turbulent Boundary Layer and Near Wake of a Low-Drag Body of Revolution.," Institute of Hydraulic Research University of Iowa, IIHR Report No. 210, 1977.
[45] Arntz, A., Atinault, O., and Merlen, A., "Exergy-Based Formulation for Aircraft Aeropropulsive Performance Assessment: Theoretical Development," *AIAA Journal*, Vol. 53, No. 6, 2015, pp. 1627–1639. https://doi.org/10.2514/1.J053467